The role of defects on the performance of quantum dot intermediate band solar cells

L. J. COLLAZOS, M. AL HUWAYZ, R. JAKOMIN, D. N. MICHA, L. D. PINTO, R. M. S. KAWABATA, M. P. PIRES, M. HENINI AND P. L. SOUZA

***Abstract*—Electrically active defects present in three InAs/GaAs quantum dots intermediate band solar cells grown by MOVPE have been investigated. The devices' structures are almost identical, differing only in the growth temperature and thickness of the GaAs layers that cover each InAs quantum dot layer. These differences induce significant changes in the solar energy conversion efficiency of the photovoltaic cells, as previously reported. In this work, a systematic investigation was carried out using Deep Level Transient Spectroscopy (DLTS) and Laplace DLTS measurements on control samples and solar cell devices, which have clearly shown that electrically active traps play an important role on the device figures of merit, such as open circuit voltage, short circuit current and shunt resistance. In particular, it was found that the well-known EL2 defect negatively affects both the open circuit voltage and shunt resistance, more in structures containing quantum dots, as a consequence of the temperature cycle required to deposit them. Other unidentified defects, that are absent in samples in which the quantum dots were annealed at 700 °C, contribute to a reduction of the short circuit current, as they increase the Shockley-Read-Hall recombination. Photoluminescence results further support the DLTS based assignments.**

***Index Terms*—Point defects, Quantum dots, Intermediate band solar cell, DLTS, Power conversion efficiency, Non-radiative recombination, MOVPE growth.**

I. INTRODUCTION

The intermediate band solar cell (IBSC) is a very attractive photovoltaic concept proposed by Luque and Marti [1], [2] to overcome the traditional Shockley-Queisser efficiency limit [3] of ~40% in a single junction solar cell (1J-SC) reaching, in principle, a maximum efficiency of 63% under solar radiation concentration [4]. In the IBSC proposal an energy band is introduced within the semiconductor material bandgap of the active layer, allowing subbandgap absorption, increasing, in turn, the short circuit current (I_{sc}), without significantly reducing the open circuit voltage (V_{oc}). A fraction of the photons of the solar spectrum with energy below the matrix material bandgap is absorbed, promoting electrons from the valence band to the intermediate band, and from the intermediate band to the conduction band, thereby enhancing I_{sc}, while the V_{oc} remains determined, essentially, by the matrix material bandgap. However, the experimentally obtained efficiencies for IBSCs are still very far from the theoretically predicted values, although much progress has been achieved in the past years [1], [2], [5], [6]. The intermediate band can be formed in various ways, for instance, with the introduction of a high concentration of impurities [7], [8] or, as it has been most often reported, by using quantum dot (QD) layers [9], where the electronic ground state of the QDs forms the intermediate band. In the case of quantum dot intermediate band solar cells (QD-IBSCs), InAs quantum dots embedded in GaAs layers have been widely investigated as a probe system. The optical

Manuscript submitted on November 18, 2020. This work was supported by CNPq (Grants 140654/2014-3, 201118/2016-5, and 153755/2016-4), FAPERJ, CAPES, and FINEP Brazilian organizations.

L. J. Collazos was with LabSem - Pontifícia Universidade Católica do Rio de Janeiro, Rio de Janeiro, Rua Marquês de São Vicente 225, CEP: 22451-900, Brazil. She is now with Centro Brasileiro de Pesquisas Físicas CBPF, Rio de Janeiro, Rua Dr. Xavier Sigaud 150, CEP: 22290-180, Brazil (e-mail: lcollazospaz@gmail.com).

M. A. Huwayz is with the School of Physics and Astronomy, University of Nottingham, University Park, Nottingham, NG7 2RD, UK, and also with the Physics Department, Faculty of Science, Princess Nourah Bint Abdulrahman University, Riyadh, Saudi Arabia (e-mail: Maryam.Alhuwayz@nottingham.ac.uk).

R. Jakomin is with Universidade Federal do Rio de Janeiro, Campus Duque de Caxias, Estrada de Xerém 27, CEP: 25245390, Brazil, and also with Instituto Nacional de Ciência e Tecnologia de Nanodispositivos Semicondutores DISSE, Rio de Janeiro, Rua Marquês de São Vicente 225, CEP: 22451-900, Brazil (e-mail: robertojakomin@xerem.ufrj.br).

D. N. Micha is with Centro Federal de Educação Tecnológica Celso Suckow da Fonseca, Campus Petrópolis, Petrópolis, Rua do Imperador 971, CEP: 25620-003, Brazil, and also with Instituto Nacional de Ciência e Tecnologia de Nanodispositivos Semicondutores DISSE, Rio de Janeiro, Rua Marquês de São Vicente 225, CEP: 22451-900, Brazil (e-mail: daniel.micha@cefet-rj.br).

L.D. Pinto, R. M. S. Kawabata, and P. L. Souza are with LabSem - Pontifícia Universidade Católica do Rio de Janeiro and Instituto Nacional de Ciência e Tecnologia de Nanodispositivos Semicondutores DISSE, Rio de Janeiro, Rua Marquês de São Vicente 225, CEP: 22451-900, Brazil (e-mails: dornnelas@yahoo.com.br; rudykawa@gmail.com; plustoza@cetuc.puc-rio.br).

M. P. Pires is with Instituto de Física, Universidade Federal do Rio de Janeiro, Rio de Janeiro, Av. Athos da Silveira Ramos 149, CEP: 21941-972, Brazil, and also with Instituto Nacional de Ciência e Tecnologia de Nanodispositivos Semicondutores DISSE, Rio de Janeiro, Rua Marquês de São Vicente 225, CEP: 22451-900, Brazil (e-mails: pires@if.ufrj.br).

M. Henini is with the School of Physics and Astronomy, University of Nottingham, University Park, Nottingham, NG7 2RD, UK (e-mail: mohamed.henini@nottingham.ac.uk).

transition energies this system provides are not the most appropriate for maximum energy conversion efficiency, but, since its growth is in a somewhat more mature stage [10], QD-IBSCs with figures of merit equal or better than an equivalent cell without the intermediate band have already been reported [11]-[16]. Several issues, which could be responsible for the cell efficiencies being short of the expected values, have been widely discussed in the literature. The escape of electrons from the IB due to tunneling or/and thermal excitation to the barrier material not only limits the required absorption from the IB to the conduction band, but also reduces V_{oc} [17]-[19]. The need of multiple QD stacks (> 20 QD layers) for a reasonable absorption volume can lead to an accumulation of misfit strain, which may trigger stacking faults and dislocation formation [20]-[22]. Another possible reason for the limited efficiency achieved so far is the presence of electrically active defects [23]. However, to the best of our knowledge, there has been no reports on their presence in QD-IBSCs and their relation to the device performance.

Recently, it has been established by Schmieder *et. al.* [24] that in GaAs solar cells the presence of the EL2 defect (an As_{Ga} antisite associated with another point defect [25]-[28]) hinders the solar cell efficiency. It is well-known that low growth temperatures favor this defect formation [25], [29], but Schmieder *et. al.* have also shown that the desired high growth rates also lead to higher EL2 densities [24]. In a similar way, Linares *et. al.* [8] attributed the very low sub-bandgap absorption in GaAs:Ti IBSCs to an excess presence of As antisites and Ga vacancies due to the low growth temperatures required to produce an appropriate Ti density. In the case of QD-IBSCs, the question which remains open is if the insertion of QD layers to fabricate IBSCs is responsible for the additional introduction of electrically active defects, which can further limit the efficiency of these devices. In this work, we have investigated the presence of electrically active defects in InAs/GaAs QD-IBSCs using deep level transient spectroscopy (DLTS) and Laplace DLTS. In order to distinguish the role played by the growth temperature and the insertion of the QDs in the active region of the devices, reference solar cells with the equivalent temperature growth sequence as the ones used for the fabrication of the QD-IBSCs were grown and the DLTS results were compared. Photoluminescence measurements were used to further support the conclusions drawn. The results indicate that the higher density of point defects found in the QD-IBSCs is mainly, but not solely, due to the low growth temperature required to nucleate the QDs.

II. Samples and Experimental Techniques

Three different series of structures were all grown by metalorganic vapor phase epitaxy (MOVPE) in an Aixtron AIX 200 reactor at 100 mbar on (001) GaAs substrates. Trimethylaluminum (TMAl), trimethylgallium (TMGa), trimethylindium (TMIn) and arsine (AsH_3) or tributylarsenide (TBAs) were used as aluminum, gallium, indium and arsenic sources, respectively. CBr_4 and dimethylzinc (DMZn) were used for *p*-doping, while SiH_4 was the *n*-dopant source. The first series consists of three QD-IBSC *p-i-n* structures, depicted in Fig. 1(a). The difference between the three structures resides on the growth parameters of the one μm-thick active layer. The QDs samples QD 6-630 and QD 6-700 were capped with a 6 nm thick GaAs barrier layer, while sample QD 3-700 was capped with a 3 nm thick GaAs. The QDs sample QD 6-630 was annealed at 630 ºC after being capped, while for the other two samples the QDs were annealed at 700 ºC. For all samples, the QDs were grown at 490 ºC, *n*-doped to an electronic density equal to 2 x 10^{17} cm^{-3}, deposited for 2.4 s, reaching a density estimated to be 1.8 x 10^{10} cm^{-2} and height of around 3.5 nm for the free standing calibration samples. A detailed description of the growth procedure is described elsewhere [16]. The second series consists of three similar structures, where the active layer is just GaAs with the same thickness as that of the QD-IBSC structures. These cells are labelled SC-630 and SC-700 (Fig. 1(b)), in which the active layer was grown at 630 ºC and 700 ºC, respectively, and SCycle (Fig. 1(c)) in which the active layer was grown by periodically changing the growth temperature between 490 ºC and 700 ºC, similar to the temperature cycle used for the QDs' deposition. Finally, Fig. 1(d) shows two *p*-type and two *n*-type GaAs layers which were grown at 570 ºC and 630 ºC. It is worth pointing out that, as previously reported, STEM images of the QD-IBSCs showed no evidence of plastic relaxation and threading dislocations [16]. The spacers and capping layers of the QD-IBSCs, as well as the active region layers of the solar cells without QDs, have residual *p*-doping concentrations very close to 1 x 10^{15} cm^{-3} for the used growth temperature range 500 °C to 700 °C, as determined from Hall measurements in single layers grown under the same conditions. The doping concentrations of *p*-doped samples are 6.2 x 10^{16} cm^{-3} and 1.9 x 10^{16} cm^{-3} for p570 and p630, respectively, and for the *n*-doped ones are 1.0 x 10^{16} cm^{-3} and 1.3 x 10^{17} cm^{-3} for n570 and n630, respectively.

In trying to identify, quantify and localize defects present in the QD-IBSCs acting as carrier traps, DLTS [30] and Laplace DLTS [31]-[32] measurements were performed, using a capacitance-meter Boonton 7200, a pulse generator Agilent 33220A, a temperature controller Lake Shore 331, and a cryostat Janis CCS-450. The sample temperature was varied between 20 K and 450 K at 2 K/min rate. The DLTS and LDLTS software used was developed by a joint project of University of Manchester and Institute of Physics, Polish Academy of Sciences.

For these same measurements, the samples were prepared using standard photolithography and wet chemical etching methods to fabricate electrical mesas. In order to produce a depletion layer for the capacitance measurements, Schottky diodes were produced with the single layer samples by deposition of Ti/Au (10 nm/ 160 nm) over GaAs:C or GaAs:Si (Schottky contact) and of Ge/Au/Ni/Au (30 nm/45 nm/30 nm/1.50 nm) over the back of the substrates (Ohmic contact). Meanwhile, for the QD-IBSCs and the solar cells without QDs, which are *p-i-n* junctions and already have intrinsic depletion regions, just Ohmic contacts were needed and consisted of Au/Zn/Au (15 nm/30 nm/130 nm) on the *p* top side and Ge/Au/Ni/Au (30 nm/45 nm/30 nm/1.50 nm) on the *n*-type

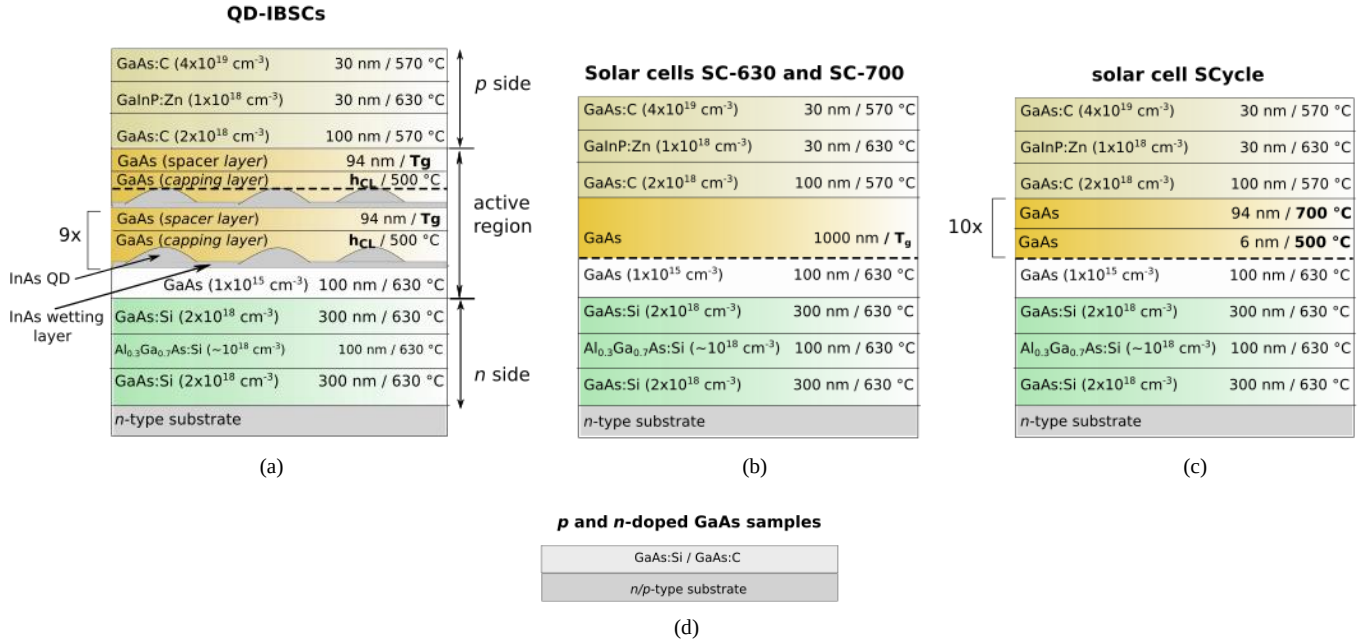

Fig. 1. Schematic diagrams showing the layer structures of the investigated samples. The black dashed line in (a), (b) and (c) shows the position of the *p*-*n* junction. $\mathbf{T_g}$ is the growth temperature (630 or 700 ºC) and $\mathbf{h_{CL}}$ refers to capping layer height (3 or 6 nm).

substrates. Solar cell current-voltage measurements under standard test illumination condition (AM1.5G, 25 ºC, and 100 mW/cm^2) were performed in mesa structures processed with 0.0547 cm^2 with a finger structure covering around 10% of the front surface. The other 90% was covered with a double layer anti-reflective coating composed of MgF_2/Ta_2O_5 (80 nm/60 nm).

In DLTS measurements, modulated by a reverse bias pulse, the consequent change in the capacitance of the sample due to the thermally excited escape of carriers from traps allows one to determine the different trap concentrations (using (1) and (2)) which take into account the effective region within the charge depletion region contributing to the carrier emission [33]:

$$N_T = 2N_d\frac{\Delta C_0}{C_2}\frac{W^2(V_r)}{[(W(V_r)-\Lambda)^2-(W(0)-\Lambda)^2]} \quad (1)$$

with

$$\Lambda = \left[\frac{2\varepsilon}{q^2N_d}(E_F-E_T)\right]^{1/2} \quad (2)$$

where ε is the dielectric permittivity of the material, q is the electronic charge, N_d is the doping concentration of the sample, ΔC_0 the DLTS peak height, C_2 the steady-state capacitance at reverse voltage (V_r), $W(V_r)$ and $W(0)$ represent the depletion depth at V_r and zero bias, respectively, and Λ is the portion of the depletion not contributing to the carrier emission, which in turn, depends on the Fermi energy level (E_F) and the trap energy (E_T) within the GaAs band gap. Moreover, Laplace DLTS provides the fingerprints of the different carrier traps, namely their capture cross section (σ) and their activation energy (ΔE_T), *i.e.* the trap energy level with respect to the energy band involved in the capture/emission process. Equation (3) provides the basis of Laplace DLTS, in which the trap emission rate, e, is related to the trap cross section and activation energy:

$$e = Am_e{}^*\sigma T^2 exp[-\Delta E_T/K_BT] \quad (3)$$

where A is a temperature independent constant, m_e* the majority carrier effective mass, K_B the Boltzmann constant, and T the sample temperature. PL spectra were obtained at temperatures varying from 20 K to 290 K, using the 532 nm line of an Nd:YAG laser with various power densities as excitation and a 250 mm monochromator coupled to a germanium nitrogen-cooled photodetector connected to a lock-in amplifier for synchronous detection.

Note that the DLTS measurements are performed under reverse bias to induce an appreciable depletion region and the solar cell operates with illumination and under forward bias, leading to changes in the relevant Fermi levels, which may modify the role of traps in the device performance. However, despite this difference, as it will be shown later, there is strong evidence that the detected traps remain active in the solar cells under operation conditions since a correlation is obtained between trap density and deterioration of cell performance.

III. DLTS AND LAPLACE DLTS RESULTS

Figs. 2 (a) and (b) show the DLTS signal for the single *p* and *n* layers, respectively, obtained under a 1 ms-single reverse bias pulse (-1 V --> 0 V --> -1 V) and using a 200 s^{-1} rate window. The identification of traps in such layers is important because

equivalent layers are part of the QD-IBSCs. All the observed defects are majority carrier traps since the peaks are all positive. The DLTS spectra have been fitted with Gaussian curves, as shown by the dotted lines in Figs. 2 (a) and (b). For the *p*-doped samples, two DLTS peaks are detected, α and β, for the sample grown at 630 ºC and two others, γ and *I*, for the sample grown at 570 ºC. Applying the Laplace DLTS to the *p* layers, the Arrhenius curves shown in Fig. 2(c) are obtained. Due to low signal to noise ratio it was not possible to obtain a clear curve for trap *I*. Trap β, with an activation energy ΔE_T = 0.86 eV and σ = 6 x 10^{-13} cm^2, has a concentration equal to 1.1 x 10^{14} cm^{-3}, obtained using (1) and (2). It is possible that trap *I*, present in sample p570 and observed at the same temperature as trap β, is the same one, however, we cannot confirm, since it was not possible to determine its fingerprints. Trap γ, with ΔE_T, σ and concentration equal to 0.33 eV, 8.5 x 10^{-19} cm^2 and 7.3 x 10^{13} cm^{-3}, respectively, despite having an activation energy and a cross section compatible with hole trap HMC [34], it was not possible to unambiguously attribute it to such defect. Its emission rate dependency on electric field, according to the Frenkel-Poole effect [35], was not observable with the available data. The hole trap, α, with ΔE_T, σ and concentration equal to 0.59 eV, 3.7 x 10^{-15} cm^2 and 3.4 x 10^{14} cm^{-3}, respectively, even though it could also not be precisely identified, should be related to the presence of C, as it will be shown later. These trap parameters, together with the errors involved in the fitting procedure, are shown in Table I.

The two *n*-doped samples present one well-defined DLTS peak each at around 390 K, which were clearly observed in the Laplace DLTS, as shown in Fig. 2(d). The peak labelled ε with ΔE_T = 0.81 eV, σ = 1 x 10^{-13} cm^2 and concentration of 1.2 x 10^{14} cm^{-3} is identified as the EL2 defect [25]-[28]. Such EL2 concentration is of the same order of magnitude, as previously reported for MOVPE grown samples [36]. Trap δ, with a concentration of the order of 2.4 x 10^{14} cm^{-3}, ΔE_T = 0.67 eV and σ = 5 x 10^{-15} cm^2 remains unidentified.

Since the solar cell samples are *p*-*i*-*n* structures composed of different layers, it is of paramount importance to determine, through capacitance measurements, the size of the depletion layer for different applied reverse biases. With such information, the reverse bias can be chosen such that the probed depleted area is within the active region of the solar cell. Meaningful comparisons between the data obtained from different samples can then be made. Fig. 3(a) shows the variation of the depletion width as a function of reverse bias for the solar cells without QDs. For applied reverse bias between -2 and -3 V (voltage range used in the DLTS measurements), samples SC-630 and SC-700 have a depletion layer width of about 900 nm, which corresponds to about 82% of the intrinsic region, while for SCycle, it is about 62%.

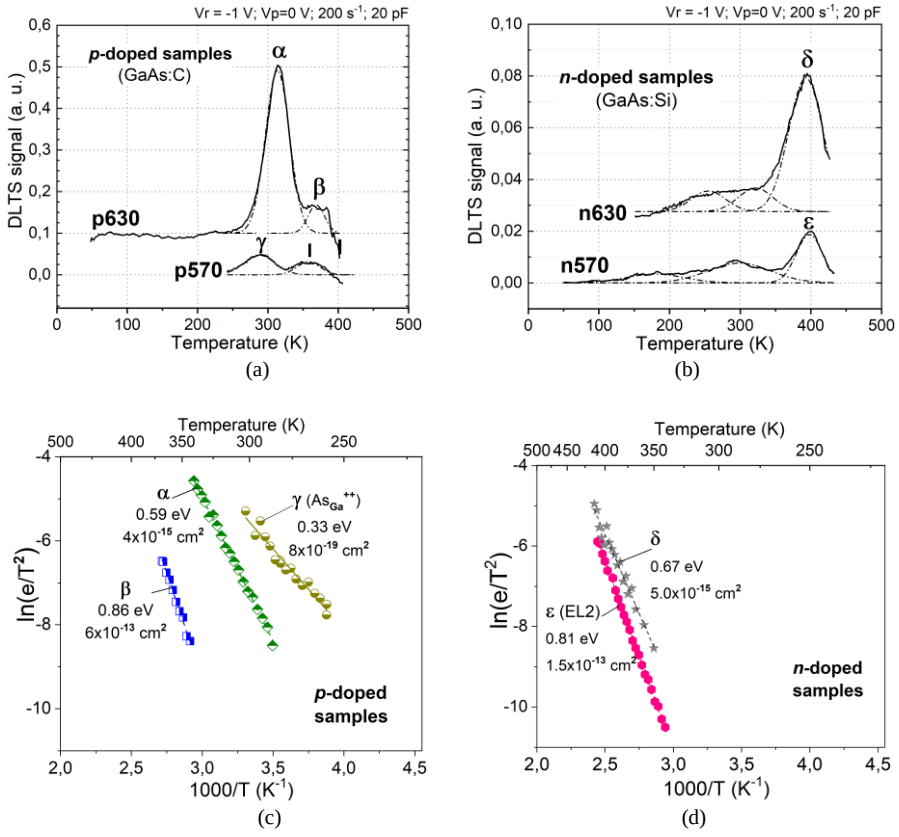

Fig. 2. DLTS spectra of (a) *p* and (b) *n*-type single GaAs layers and (c-d) their corresponding Arrhenius plots extracted from Laplace DLTS measurements. These spectra were obtained by applying reverse bias pulses V_r --> V_p --> V_r, as detailed on the DLTS graphs. The signatures of the detected traps (ΔE_T and σ) are shown on the Arrhenius plots.

TABLE I

DETAILS OF THE HOLE AND ELECTRONS TRAPS DETECTED IN THE p AND n-TYPE GaAs LAYER SAMPLES (ΔE_T: THERMAL ACTIVATION ENERGY; σ: CAPTURE CROSS-SECTION; N_T: TRAP CONCENTRATION). THE SYMBOLS (+) AND (-) NEXT TO THE TRAP ASSIGNED LETTERS DENOTE IF THEY ARE HOLE OR ELECTRON TRAPS, RESPECTIVELY. THE ERRORS OF ΔE_T AND σ RESULT FROM THE LINEAR REGRESSION OF THE RESPECTIVE ARRHENIUS CURVES, WHILE THE ERROR SHOWN FOR N_T WERE DEDUCED FROM THE GAUSSIAN FIT OF THE DLTS PEAKS.

Sample	Trap	ΔE_T (eV)	σ (10^{-15} cm^2)	N_T (10^{14} cm^{-3})	Identity
p570	γ (+)	0.33 ± 0.02	0.00085 ± 0.00066	0.73 ± 0.05	As_{Ga}^{++}
p630	α (+)	0.59 ± 0.01	3.7 ± 1.0	3.4 ± 0.2	unidentified
	β (+)	0.86 ± 0.02	580 ± 450	1.1 ± 0.1	unidentified
n570	ε (-)	0.81 ± 0.01	150 ± 30	1.2 ± 0.1	EL2
n630	δ (-)	0.67 ± 0.03	5.0 ± 4.5	2.4 ± 0.1	unidentified

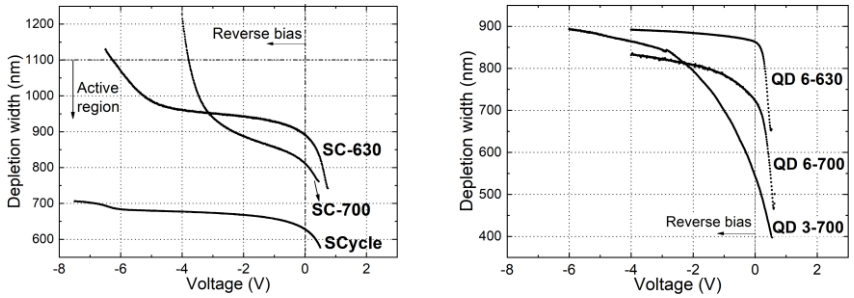

Fig. 3. Charge depletion width of (a) the solar cells without QDs and (b) the QD-IBSCs as a function of the reverse voltage V_r, calculated from capacitance-voltage measurements, where the parallel capacitance model has been used.

It should be noted that the intrinsic regions are, in fact, slightly *p*-type due to residual C doping found in MOVPE grown samples. In the case of QD-IBSCs, shown in Fig. 3(b), where the QDs in the intrinsic region are *n*-doped, the depletion width varies between 675 nm and 900 nm for the three samples. However, in the same -2 to -3 V reverse bias voltage range, the depletion layer corresponds to about 73 to 82% of the active layer.

The DLTS signal for the solar cell samples without QDs is shown in Fig. 4(a), where two hole traps (positive peaks due to majority carriers), peaks α and β, can be observed around 320 K and 420 K, respectively, for all samples and one electron trap (negative peak due to minority carriers) around 250 K is detected in sample SC-630. The corresponding Arrhenius plots obtained by Laplace DLTS are depicted in Fig. 4(b). Peak α in samples SC-700 and SCycle has the same signature, ΔE_T and σ, as in the single *p*-doped layer grown at 630 ºC. For sample SC-630, where an electron trap η is present, one observes a change in ΔE_T and σ, even though the DLTS signal is observed at the same temperature as in the other two samples. It is believed that the presence of trap η induces a difficulty in extracting the data from the Laplace DLTS plots. Therefore, we consider peak α, in all SC samples, to be the same unidentified defect observed in the p630 sample. Additionally, except for sample SC-700, essentially the same trap concentration (2.3 x 10^{14} cm^{-3}) is determined. For sample SC-700, which was subjected to a temperature of 700 ºC, the α trap concentration was reduced by one order of magnitude, demonstrating that this defect was partially annealed out. This trap remains unidentified, but it should be related to the presence of the residual C dopant, since the same trap is present in the *p*-doped sample with a concentration 50% higher. The electron trap η, with ΔE_T = 0.25 eV and σ = 2.4 x 10^{-19} cm^2, has a cross section four orders of magnitude lower than the other detected traps and has not been detected in the *n*-doped layers, behaving in the SC-630 sample as a minority carrier trap. Peak β has the same fingerprints of the hole trap already discussed for the *p*-doped layers, therefore it can be attributed to the same unidentified type of defect.

The analysis of the three QD-IBSC samples is discussed below. Fig. 5(a) shows the DLTS signal for the QD-IBSC QD 6-630 for -1 V and -3 V bias, where the data have been fitted with Gaussian curves, while the Arrhenius plots corresponding to the different traps detected by the Laplace DLTS are depicted in Fig. 5(b). Note that the active region of the QD-IBSCs have been *n*-doped, therefore the observed peaks are electron traps. As in the single *n*-type GaAs layers, we observe the presence of the EL2 trap, with the corresponding fingerprints, here labelled ε. However, here we detect four other different peaks κ, λ, *E1* and *E2*, which are not present neither in the single GaAs layers nor in the solar cells without quantum dots, therefore they should be a consequence of the presence of the QDs. Peaks named *U1* and *U2* in Fig. 5(a) were not discernible in the Laplace DLTS data.

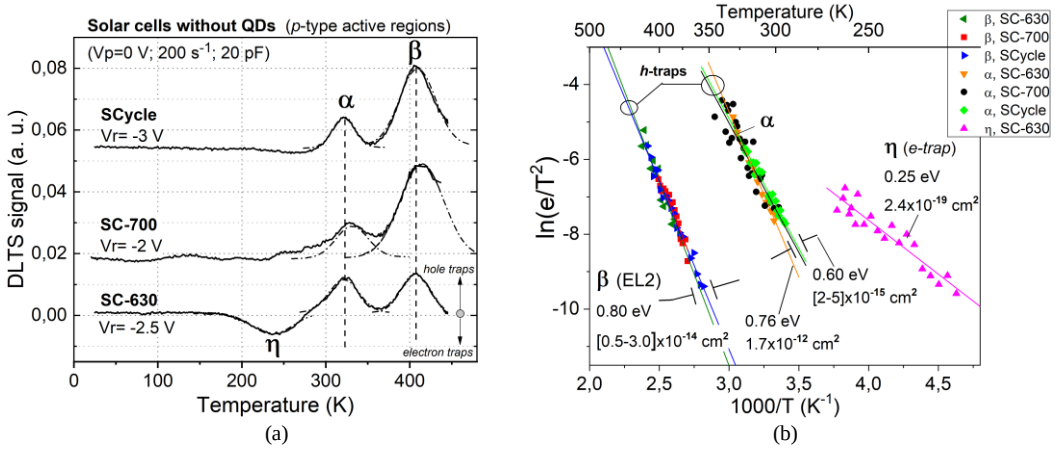

Fig. 4. (a) DLTS spectra and (b) Arrhenius plots of the solar cells without QDs, obtained under different reverse bias pulses, as detailed on the DLTS graph. The arrows on the DLTS graph indicate which peaks correspond to electron or hole traps according to their direction. The electrons and hole traps are identified as *e*-traps and *h*-traps in the Arrhenius plots.

The electron trap κ with ΔE_T = 0.30 eV and σ = 2.0 x 10^{-18} cm^2 is only present in the QD-IBSC sample annealed at 630 °C, therefore it should be related to the insertion of the quantum dots, however, its nature has not been identified. Electron trap λ with ΔE_T = 0.58 eV, σ = 1.4 x 10^{-15} cm^2 and a concentration equal to 4.3 x 10^{15} cm^{-3}, is tentatively attributed to the field dependent M3 defect, which is one of the metastable configurations of a defect identified as a pairing of a native acceptor or defect complex (c^-) and a shallow donor (d^+), observed in MOVPE grown *n*-GaAs layers [37]. The shallow donor would be the Si used to dope the QDs, which could diffuse into the GaAs layer around it. The native acceptor or defect complex could be induced by the presence of strain fields around the QDs, which extend to the GaAs surrounding layers and are typical of the InAs/GaAs QD systems [20]. This trap, like trap κ, is associated with the presence of the quantum dots.

The DLTS signals *E1* and *E2* have very low activation energies ΔE_T equal to 0.19 eV and 0.16 eV, respectively, and very small capture cross sections σ in the range 2 x 10^{-20} cm^2 and 4 x 10^{-19} cm^2. The activation energies are compatible with electron thermal emission from confined states in InAs QDs embedded in GaAs [38]. Indeed, calculations of the band structure performed with the Nextnano software [39], for our InAs/GaAs system at room temperature, have provided transition energies from the electronic ground state and first excited state of the InAs QD to the bottom of the GaAs conduction band. Values in the range 0.15-0.21 eV, for QD heights between 2 and 6 nm (in QD 6-630 and QD 6-700 samples), and 0.13-0.15 eV, for heights between 2 and 3 nm (in QD 3-700 sample), were obtained, in excellent agreement with the determined activation energies ΔE_T from the DLTS measurements. Thus, these two DLTS signals reveal, in fact, the electronic confined states. Further support for such assignment is found with a simple estimation. The *E1* and *E2* concentrations are 4.0 x 10^{15} cm^{-3} and 4.4 x 10^{15} cm^{-3}, respectively, with a standard deviation around ± 20%. If the density of ground (corresponding to *E1*) and first excited (corresponding to *E2*) states available for emission are determined from the QD density, the volume it occupies and the levels degeneracy, values of the order of 3.6 x 10^{15} cm^{-3} for the ground state and 7.2 x 10^{15} cm^{-3} for the first excited state are obtained, consistent with the measured "trap" density from (1).

For the IBSCs for which the QD annealing took place at 700 ºC, the DLTS data, and respective Laplace DLTS Arrhenius plots, for two reverse bias voltages each, are shown in Figs. 5(c)-(f). The striking feature is that only the trap associated with the EL2 defect is observed, indicating that traps κ and λ, associated with defects introduced by the QDs themselves have been annealed out at 700 °C. It should be pointed out that the EL2 concentration was more than one order of magnitude higher than that in the single layers, most likely due to the lower temperatures used for QD deposition [25], [29]. An increase in EL2 concentration with the introduction of InAs QDs has also been previously observed [36]. Traps κ and λ could be modified by the higher temperature due to partial release of strain, however, they are most likely present at the boundaries of the InGaAs disk formed on top of the InAs QDs during the annealing procedure [16]. At 700 ºC annealing temperature, the In migration during the In flush procedure forms a full interconnected InGaAs thin layer, instead of disks, further reducing the strain and eliminating these traps. The question, which remains, though, is why the confined states' signals, *E1* and *E2*, should be absent.

In order to tackle this question, PL measurements were carried out. The 20 K PL spectra of the three QD-IBSCs are shown in Fig. 6. Peaks B_{LT} (1.26 eV), B_{HT} (1.34 eV) and B_S (1.37 eV) correspond to the interband ground states recombination for samples QD 6-630, QD 6-700 and QD 3-700, respectively, while C_{LT} (1.31 eV) and C_{HT} (1.38 eV) are related to the equivalent first excited states recombination, such optical transition not being detected for sample QD 3-700. These assignments were based on PL measurements as a function of temperature and excitation power (data not shown here), following the method described in [40].

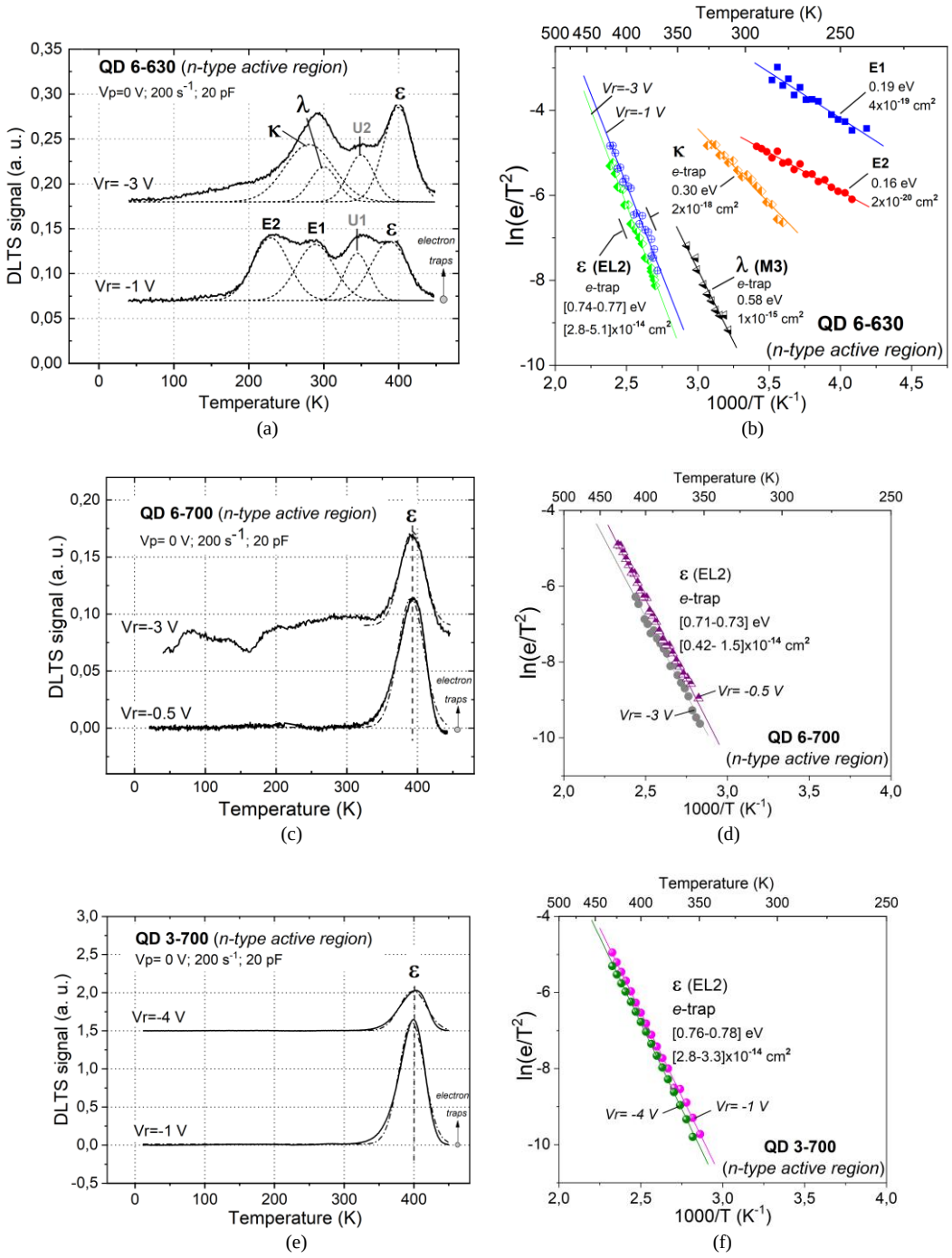

Fig. 5. (a,c,e) DLTS spectra and (b,d,f) corresponding Arrhenius plots of the QD-IBSCs samples QD 6-630, QD 6-700, and QD 3-700, respectively, obtained at two different reverse voltages V_r each, as detailed on the DLTS graph. Traps U1 and U2 were not detected by Laplace DLTS. The electrons traps are identified as *e*-traps in the Arrhenius plots. The arrows in positive direction indicate that the DLTS peaks correspond to electron traps.

The PL spectra showed a saturation of the lower energy peak emitted by the QDs with respect to the higher energy one, consistent with ground and first excited states, respectively. Additionally, as the temperature is increased a relative reduction of the PL emission at higher energy is observed due to thermal quenching, further supporting our assignments. Note that the InAs wetting layer (WL), which has a thickness of 2 ML, would give rise to a PL peak between 1.42 and 1.45 eV if no interdiffusion occurs [41]-[43]. If there is In-Ga interdiffusion, which is certainly the case for an annealing temperature of 700 ºC, then the WL peak emission would be at an even higher energy, outside the energy range shown in Fig. 6.

TABLE II
SIGNATURES AND CONCENTRATIONS OF THE TRAPS DETECTED BETWEEN -3 AND -4 V IN THE ACTIVE REGIONS OF THE IBSCS. THE VALUES FOR THE TRAPS DETECTED IN SOLAR CELL SC-700 ARE ALSO SHOWN FOR COMPARISON (ΔE_T: THERMAL ACTIVATION ENERGY; σ: CAPTURE CROSS-SECTION; N_T: TRAP CONCENTRATION). THE SYMBOLS (+) AND (-) NEXT TO THE TRAP ASSIGNED LETTERS DENOTE IF THEY ARE HOLE OR ELECTRON TRAPS, RESPECTIVELY. THE ERRORS OF ΔE_T AND σ RESULT FROM THE LINEAR REGRESSION OF THE RESPECTIVE ARRHENIUS CURVES, WHILE THE ERROR SHOWN FOR N_T WERE DEDUCED FROM THE GAUSSIAN FIT OF THE DLTS PEAKS.

Sample	Trap	ΔE_T (eV)	σ (10^{-15} cm^2)	N_T (10^{15} cm^{-3})	Identity
SC-700	α (+)	0.60 ± 0.05	1.8 ± 4.9	0.0331 ± 0.0006	unidentified
	β (+)	0.82 ± 0.06	23 ± 41	0.115 ± 0.002	unidentified
QD 6-630 (-3 V)	*E1*	0.19 ± 0.01	0.00043 ± 0.00028	4.0 ± 0.9	QD's electronic ground state
	E2	0.16 ± 0.01	0.000019 ± 0.000006	4.4 ± 0.9	QD's electronic first excited state
	κ (-)	0.30 ± 0.01	20 ± 10	6.9 ± 1.4	unidentified
	λ (-)	0.58 ± 0.04	1.4 ± 1.7	4.3 ± 0.9	M3
	ε (-)	0.77 ± 0.02	51 ± 26	12 ± 2	EL2
QD 6-700 (-3 V)	ε (-)	0.71 ± 0.02	4.2 ± 2.0	6.0 ± 0.7	EL2
QD 3-700 (-4 V)	ε (-)	0.78 ± 0.01	33 ± 7	3.0 ± 0.1	EL2

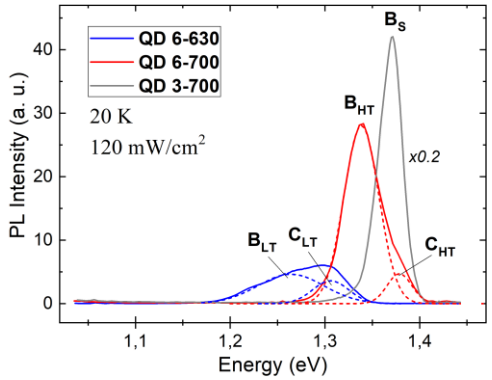

Fig. 6. 20 K-Photoluminescence spectra of the three QD-IBSCs at 120 mW/cm^2 laser excitation density. The solid and dashed curves correspond to the measured and the fitted PL spectra, respectively.

Additionally, it should be pointed out that equivalent samples with free standing dots showed a monomodal distribution of QDs in atomic force microscopy images. One notices that the transition energies are larger for the samples annealed at 700 ºC, indicating smaller QDs. The energy differences between B_{LT} and B_{HT} and between C_{LT} and C_{HT} peaks are 80 meV and 70 meV, respectively. A simple estimation of the electron escape for the samples annealed at 700 ºC can be made. Considering the conduction and valence band offsets for the InAs/GaAs system to be 70 % and 30 % [44], the electronic ground and first excited states for sample QD 6-700 should be about 0.13 eV and 0.11 eV from the GaAs conduction band, while 0.19 eV and 0.16 eV for the case of sample QD 6-630. The traps *E1* and *E2* for QD 6-700 were most likely not detected because the lower energies make it difficult for the electronic level to hold the carriers. Note that the capture cross section for *E1* and *E2* for QD 6-630 are already in the 10^{-19} to 10^{-20} cm^2 range, as shown in Fig 4(b). Since the PL ground state transition peak for sample QD 3-700 occurs for an even higher energy, it is naturally expected that this energy level is not detected by the DLTS measurements (see Fig. 5(e)). In this case, the excited state is only 80 meV from the top of the barrier, substantially increasing the electron escape probability and inhibiting the PL transition, which is not observed at 20 K. For sample QD 3-700, for which the QD capping layer is thinner, the dots' heights are limited to 3 nm, the capping layer thickness, therefore it is only natural that the dots be smaller compared to those of other samples. In the case of samples QD 6-630 and QD 6-700, the height of the QDs should, in principle, be limited to the capping layer thickness of 6 nm, however, in the case of the sample annealed at lower temperature, the excess height is not always significantly reduced, leading to a less homogeneous QD height distribution [16]. It should be pointed out that it would be more favorable for an IBSC to have a higher energy barrier for electron escape, meaning having larger QDs in order to reduce the thermal escape. It is fair to say that PL measurements and theoretical calculations indicate that levels corresponding to *E1* and *E2* are present in sample QD 6-700 and *E1* in sample QD 3-700, respectively, although not detected by the performed DLTS experiments.

The beneficial effect of the higher annealing temperature becomes even clearer when the PL intensity of the different samples are compared. The integrated PL intensity from the QDs sample QD 3-700 is about a factor of 7 and 40 larger than that of samples QD 6-700 and QD 6-630, respectively, denoting an improved optical quality of the samples. This improvement is accompanied by a monotonous decrease in the EL2 concentration, from 12.0 x 10^{15} cm^{-3} to 3.0 x 10^{15} cm^{-3}, as depicted in Table II.

The conclusion one can draw this far from the reported systematic DLTS investigation is that the defects found in the QD-IBSC are, in fact, predominantly introduced due to the low temperatures required for the deposition of the QDs, and not due to the QDs themselves and the morphological changes they impart to the solar cell structures. The presence of the EL2 trap is somewhat an exception. It is always present, however, its concentration can be lowered if low growth temperatures are not needed. The EL2 concentration detected was about 4 times

lower when the QD annealing temperature went up from 630 ºC to 700 ºC.

IV. Discussion of the Role of the Defects on the Performance of the QD-IBSCs

Fig. 7 shows the current density *versus* voltage (*J-V*) curves measured under standard test conditions (AM1.5G, 100 mW/cm^2 and 25 ºC) for the QD solar cells and for the SC-700, which is the sample without QDs and annealed at 700 ºC, and serves as the reference sample. The curves clearly show that the presence of the QDs reduce V_{oc} and the QDs' low annealing temperature significantly decreases the short circuit current density (J_{sc}). The figures of merit for these solar cells are shown in Table III. As one can infer from the current density given in (4), obtained using the solar cell equivalent circuit model, V_{oc} strongly depends on the shunt resistance (R_{SH}):

$$J = J_L - J_0\left[exp\left(\frac{qV}{nK_BT}\right) - 1\right] - \frac{V}{AR_{SH}} \quad (4)$$

where J_L is the light generated current density, J_0 the diode drift current density, n the diode ideality factor, K_B the Boltzmann constant, T the temperature and A, the area. R_{SH} times the cell area was determined from the negative of the inverse of the *J-V* curve at voltages close to J_{sc}. It was found that for the reference sample R_{SH} is around 20 times larger than that of the QD 6-630 sample. As can be seen in Table III, the larger R_{SH}, the larger V_{oc} is. Low R_{SH} indicates the presence of alternate current paths, which are attributed to defects that offer current carriers a lower energy way to recombine. The EL2 defect is present in all these QD solar cell structures and its concentration monotonously increases from zero for the reference cell to 1.2 x 10^{16} cm^{-3} for the QD 6-630 sample. A strong correlation is observed between the increase in the EL2 concentration and the reduction of both V_{oc} and R_{SH}, revealing the important role played by the EL2 trap in hindering the performance of the device. The EL2 concentration in these different solar cells is indicated in Table II. A lower V_{oc} is in fact expected for the QD-IBSC with respect to the reference [1], primarily due to partial thermal extraction of carriers from the electronic QD level, which reduces the effective bandgap of the active region. It should be noted though that the samples annealed at 700 ºC experience a larger diffusion of Ga into the InAs QDs, increasing their fundamental transition energy. However, it is estimated that this increase in transition energy would be at most 80 meV [16] far below the 250 meV needed to explain the measured increase in V_{oc}. A similar relationship between EL2 concentration and V_{oc} has already been reported for conventional solar cells grown at different growth rates [24]. In the case of QD-IBSCs this effect is further highlighted due to the low temperature intervals required for the QDs' deposition, which favors the formation of such defects, as previously mentioned. We quantitatively estimated the impact of each source of loss in V_{oc} by simulating *IV*-curves for the sample QD 3-700 (not shown here) with SCAPS [45], a drift-diffusion model solver, under different loss scenarios. Based on this analysis, it is possible to infer that an effective bandgap energy of 1.32 eV for the intrinsic layer (100 meV reduction) reduces V_{oc} by 27% (96 mV), whereas the introduction of the detected defects contributes with 73% (266 mV) to the total loss.

Note that, according to the *J-V* curve for sample QD 3-700, the slope around V_{oc} is significantly less steep than it is for the other samples, indicating a higher series resistance. One could try to associate this observation also to the investigated defects, however our data do not support such claim, because QD 3-700 presents the best figures of merit and lower defect concentration. We believe this is an artifact attributed to a processing step.

On the other hand, one notices that J_{sc} is mostly affected by the annealing temperature. The obtained result indicates that the origin for such a major reduction of J_{sc} is suppressed when the QDs are subjected to temperatures around 700 ºC. Based on the DLTS data presented before, electron traps κ and λ are, in fact, removed at this temperature, therefore, they are good candidates to be responsible for the loss in J_{sc}. A reduction in J_{sc} is most often a consequence of large Shockley-Read-Hall (*SRH*) recombination [46]. Analyzing the PL spectra shown in Fig. 6, it is clear that the integral radiative recombination is by far the lowest in the QD-IBSC device annealed at 630 ºC, which is consistent with an increased *SRH* recombination.

V. Conclusion

A systematic investigation of the role played by electrically active point defects on the performance of QD-IBSCs has been carried out. In order to identify, locate and determine the origin of the detected electrically active defects in QD-IBSCs, DLTS, Laplace DLTS, and PL techniques were used to first characterize layers that compose the investigated QD-IBSCs and conventional solar cells with equivalent structures, but without the quantum dots. The predominant defect detected in the QD-IBSCs is the EL2 trap and its concentration correlates well with the reduction of both R_{SH} and V_{oc}.

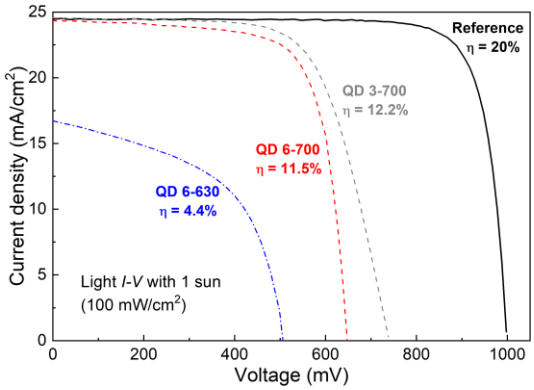

Fig. 7. Current density-voltage characteristics of the three QD-IBSCs samples, namely, QD 6-630, QD 6-700 and QD 3-700, and the reference solar cell, SC-700, with a 1 µm-GaAs active region without QDs, grown at 700°C. The respective solar energy conversion efficiencies (η) are also shown.

TABLE III
SUMMARY OF FIGURES OF MERIT OF THE IBSCS DEVICES SHOWN IN FIG. 7, INCLUDING CONVERSION EFFICIENCIES (η) AND FILL FACTORS (*FF*).

Sample	J_{SC} (mA/cm^2)	V_{OC} (V)	FF	η (%)	R_{SH} (kΩ)
Reference (SC-700)	24.4	0.998	0.82	20	35.5 ± 6.2
QD 6-630	16.8	0.511	0.52	4.4	1.81 ± 0.03
QD 6-700	24.4	0.648	0.73	11.5	8.90 ± 0.53
QD 3-700	24.1	0.738	0.67	12.2	31.0 ± 3.2*

*The fitting of the *IV*-curve for this sample was performed using a lower voltage range (from 0 to 500 mV) to avoid the part of the curve in which the high series resistance has the major influence ($V \rightarrow V_{OC}$).

Comparing the J_{sc} for the investigated QD-IBSCs with that of the reference sample, only the one annealed at 630 ºC showed a significant reduction. Such decrease is tentatively attributed to the defects, labelled here κ and λ. The origin of the former could not be identified and the latter was attributed to the known M3 defect, being both traps annealed out at 700 ºC.

It is clear from our results that the presence of electrically active defects, in relatively high concentrations ($\geq 10^{15}$ cm^{-3}), hinders the figures of merit of the solar cells. In the case of QD-IBSCs or any quantum dot solar cell, the required low temperatures for the deposition of the QDs is the major limitation since it favors the nucleation of such defects.

ACKNOWLEDGMENT

The authors would like to thank one of the unknown reviewers for bringing up the point of comparing the QDs density of states with the concentration of traps E1 and E2. We acknowledge the processing steps and measurements made at Fraunhofer ISE, in Germany, performed by Elisabeth Schaefer and Rita M. S. Freitas, and the support of Vera Klinger and Frank Dimroth. The authors also especially acknowledge Stefan Birner and the Nextnano staff for all the support and help. M. Henini and M. A. Huwayz are grateful for the support by a grant from the deanship of scientific research, Princess Nourah Bint Abdulrahman University, Riyadh, KSA. The project was partially supported by CAPES, FAPERJ (E-26/010.000980/2019), CNPq and FINEP.

REFERENCES

[1] A. Luque, and A. Martí, "The intermediate band solar cell: progress toward the realization of an attractive concept," *Adv. Mater*., vol. 22, no. 2, pp. 160-174, Jan. 2010.

[2] A. Luque, A. Martí, and C. Stanley, "Understanding intermediate-band solar cells," *Nat. Photonics*, vol. 6, no. 3, pp. 146-152, Feb. 2012.

[3] W. Shockley and H. J. Queisser, "Detailed balance limit of efficiency of *p-n* junction solar cells," *J. Appl. Phys*., vol. 32, no. 3, pp. 510-519, 1961.

[4] A. Luque and A. Martí, "Increasing the efficiency of ideal solar cells by photon induced transitions at intermediate levels," *Phys. Rev. Lett.*, vol. 78, no. 26, pp. 5014, Jun.1997.

[5] Y. Okada, N. Ekins-Daukes, T. Kita, R. Tamaki, M. Yoshida, A. Pusch, O. Hess, C. Phillips, D. Farrell, K. Yoshida, N. Ahsan, Y. Shoji, T. Sogabe, and J.-F. Guillemoles, "Intermediate band solar cells: Recent progress and future directions," *Appl. Phys. Rev.*, vol. 2, no. 2, pp. 021302, Apr. 2015.

[6] I. Ramiro and A. Martí, "Intermediate band solar cells: Present and future," *Prog. Photovoltaics*, pp. 1-9, Oct. 2020.

[7] G. González-Díaz, J. Olea, I. Mártil, D. Pastor, A. Martí, E. Antolín, and A. Luque, "Intermediate band mobility in heavily titanium-doped silicon layers," *Sol. Energ. Mat. Sol. C.*, vol. 93, no. 9, pp. 1668-1673, Sept. 2009.

[8] P. Linares, A. Martí, E. Antolín, I. Ramiro, E. López, E. Hernández, D. F. Marrón, I. Artacho, I. Tobías, P. Gérard, et al., "Extreme voltage recovery in GaAs:Ti intermediate band solar cells," *Sol. Energ. Mat. Sol. C.*, vol. 108, pp. 175-179, Jan. 2013.

[9] A. Martí, E. Antolín, E. Cánovas, N. López, P. Linares, A. Luque, C. Stanley, and C. Farmer, "Elements of the design and analysis of quantum-dot intermediate band solar cells," *Thin Solid Films*, vol. 516, no. 20, pp. 6716-6722, Aug. 2008.

[10] D. Bimberg, M. Grundmann, and N. N. Ledentsov, *Quantum dot heterostructures*. John Wiley & Sons, 1999.

[11] S. M. Hubbard, C. G. Bailey, C. D. Cress, S. Polly, J. Clark, D. V. Forbes, R. P. Raffaelle, S. G. Bailey, and D. M. Wilt, "Short-circuit current enhancement of GaAs solar cells using strain compensated InAs quantum dots," in *2008 33rd IEEE Phot. Spec. Conf., IEEE*, San Diego, CA, USA, 2008, pp. 1-6.

[12] C. G. Bailey, D. V. Forbes, R. P. Raffaelle, and S. M. Hubbard, "Near 1 V open circuit voltage InAs/GaAs quantum dot solar cells," *Appl. Phys. Lett*., vol. 98, no. 16, pp. 163105, Apr. 2011.

[13] C. G. Bailey, D. V. Forbes, S. J. Polly, Z. S. Bittner, Y. Dai, C. Mackos, R. P. Raffaelle, and S. M. Hubbard, "Open-circuit voltage improvement of InAs/GaAs quantum-dot solar cells using reduced InAs coverage," *IEEE J. Photovolt*., vol. 2, no. 3, pp. 269-275, Jul. 2012.

[14] D. Guimard, R. Morihara, D. Bordel, K. Tanabe, Y. Wakayama, M. Nishioka, and Y. Arakawa, "Fabrication of InAs/GaAs quantum dot solar cells with enhanced photocurrent and without degradation of open circuit voltage," *Appl. Phys. Lett*., vol. 96, no. 20, pp. 203507, May 2010.

[15] W.-S. Liu, H.-M. Wu, F.-H. Tsao, T.-L. Hsu, and J.-I. Chyi, "Improving the characteristics of intermediate-band solar cell devices using a vertically aligned InAs/GaAsSb quantum dot structure," *Sol. Energ. Mat. Sol. C*., vol. 105, pp. 237-241, Oct. 2012.

[16] E. Weiner, R. Jakomin, D. Micha, H. Xie, P.-Y. Su, L. Pinto, M. Pires, F. Ponce, and P. Souza, "Effect of capping procedure on quantum dot morphology: Implications on optical properties and efficiency of InAs/GaAs quantum dot solar cells," *Sol. Energ. Mat. Sol. C*., vol. 178, pp. 240-248, May 2018.

[17] E. Antolin, A. Marti, P. G. Linares, I. Ramiro, E. Hernández, C. Farmer, C. Stanley, and A. Luque, "Advances in quantum dot intermediate band solar cells, in *2010 35th IEEE Phot. Spec. Conf., IEEE*, Honolulu, HI, USA, 2010, pp. 000065-000070.

[18] D. Sellers, S. Polly, S. Hubbard, and M. Doty, "Analyzing carrier escape mechanisms in InAs/GaAs quantum dot p-i-n junction photovoltaic cells," *Appl. Phys. Lett*., vol. 104, no. 22, pp. 223903, Jun. 2014.

[19] E. Antolín, A. Martí, C. Farmer, P. Linares, E. Hernández, A. Sánchez, T. Ben, S. Molina, C. Stanley, and A. Luque, "Reducing carrier escape in the InAs/GaAs quantum dot intermediate band solar cell," *J. Appl. Phys*., vol. 108, no. 6, pp. 064513, Sept. 2010.

[20] A. Martí, N. Lopez, E. Antolin, E. Canovas, A. Luque, C. Stanley, C. Farmer, and P. Diaz, "Emitter degradation in quantum dot intermediate band solar cells," *Appl. Phys. Lett*,. vol. 90, no. 23, pp. 233510, Jun. 2007.

[21] N. E. Gorji, "A theoretical approach on the strain-induced dislocation effects in the quantum dot solar cells," *Sol. Energy*, v. 86, n. 3, p. 935-940, Mar. 2012.

[22] R. Jakomin, R. Kawabata, R. Mourão, D. Micha, M. Pires, H. Xie, A. Fischer, F. Ponce, and P. Souza, "InAs quantum dot growth on $Al_xGa_{1-x}As$ by metalorganic vapor phase epitaxy for intermediate band solar cells," *J. Appl. Phys*., vol. 116, no. 9, pp. 093511, Sept. 2014.

[23] A. Luque, A. Martí, E. Antolín, and C. Tablero, "Intermediate bands versus levels in non-radiative recombination," *Physica B*, vol. 382, no. 1-2, pp. 320-327, Jun. 2006.

[24] K. J. Schmieder, E. A. Armour, M. P. Lumb, M. K. Yakes, Z. Pulwin, J. Frantz, and R. J. Walters, "Effect of growth temperature on GaAs solar cells at high MOCVD growth rates," *IEEE J. Photovolt*., vol. 7, no. 1, pp. 340-346, Jan. 2017.

[25] H. Von Bardeleben, D. Stievenard, D. Deresmes, A. Huber, and J. Bourgoin, "Identification of a defect in a semiconductor: EL2 in GaAs," *Phys. Rev. B*, vol. 34, no. 10, pp. 7192, Nov. 1986.

[26] B. Meyer, D. Hofmann, J. Niklas, and J.-M. Spaeth, "Arsenic antisite defect As_{Ga} and EL2 in GaAs," *Phys. Rev. B 36*, vol. 36, no. 2, pp. 1332, Jul. 1987.

[27] M. Kaminska and E. R. Weber, "EL2 defect in GaAs," in *Imperfections in III/V Materials, Semiconductors and Semimetals*, vol. 38, Boston, USA: Academic Press, 1993, pp. 59-89.

[28] J. Bourgoin, H. Von Bardeleben, and D. Stievenard, "Native defects in gallium arsenide," *J. Applied Phys*., vol. 64, no. 9, pp. R65-R92, Jul. 1988.

[29] J. Muszalski, A. Babiński, K. Korona, E. Kamińska, A. Piotrowska, M. Kamińska, and E. Weber, "First TSC and DLTS measurements of low temperature GaAs," *A Phys. Pol. A*, vol. 80, pp. 413-416, 1991.

[30] D. Lang, "Deep-level transient spectroscopy: A new method to characterize traps in semiconductors," *J. Appl. Phys*., vol. 45, no. 7, pp. 3023-3032, Jul. 1974.

[31] L. Dobaczewski, P. Kaczor, I. Hawkins, and A. Peaker, "Laplace transform deep-level transient spectroscopic studies of defects in semiconductors," *J. Appl. Phys*., vol. 76, no. 1, pp. 194-198, Jul. 1994.

[32] L. Dobaczewski, A. Peaker, and K. Bonde Nielsen, "Laplace-transform deep-level spectroscopy: The technique and its applications to the study of point defects in semiconductors," *J. Appl. Phys*., vol. 96, no. 9, pp. 4689-4728, Nov. 2004.

[33] D. Stievenard and D. Vuillaume, "Profiling of defects using deep level transient spectroscopy," *J. Appl. Phys*., vol. 60, no. 3, pp. 973-979, Aug. 1986.

[34] P. J. Wang, T. F. Kuech, M. A. Tischler, P. Mooney, G. Scilla, and F. Cardone, "Deep levels in p-type GaAs grown by metalorganic vapor phase epitaxy," *J. Appl. Phys*., vol. 64, no. 10, pp. 4975-4986, Nov. 1988.

[35] J. Bourgoin and M. Lannoo, *Point Defects in Semiconductors II: Experimental Aspects*, Berlin, Germany: Springer, 1983, pp. 199-201.

[36] S. I. Sato, K. J. Schmieder, S. M. Hubbard, D. V. Forbes, J. H. Warner, T. Ohshima, and R. J. Walters, "Defect characterization of proton irradiated GaAs pn-junction diodes with layers of InAs quantum dots," *J. Appl. Phys.*, vol. 119, no. 18, pp. 185702, May 2016.

[37] W. R. Buchwald, N. M. Johnson, and L. P. Trombetta, "New metastable defects in GaAs," *Appl. Phys. Lett*., vol. 50, no. 15, pp. 1007-1009, Apr. 1987.

[38] O. Engström, M. Kaniewska, Y Fu, J. Piscator, and M. Malmkvist, "Electron capture cross sections of InAs/GaAs quantum dots," *Appl. Phys. Lett*., vol. 85, no. 14, pp. 2908-2910, Oct. 2004.

[39] S. Birner, T. Zibold, T. Andlauer, T. Kubis, M. Sabathil, A. Trellakis, and P. Vogl, "Nextnano: general purpose 3-D simulations," *IEEE T. Electron Dev*., vol. 54, no. 9, pp. 2137-2142, Sept. 2007.

[40] J.-M- Gérard, O. Cabrol and B. Sermage, "InAs quantum boxes: Highly efficient radiative traps for light emitting devices on Si," *Appl. Phys. Lett.*, vol. 68, no 22, pp.3123-3125, May 1996.

[41] G. Torelly, R. Jakomin, L. D. Pinto, M. P. Pires, J. Ruiz, P. G. Caldas, R. Prioli, H. Xie, F. A. Ponce, and P. L. Souza, "Early nucleation stages of low density InAs quantum dots nucleation on GaAs by MOVPE," *J. Cryst. Growth*, vol. 434, pp. 47-54, Jan. 2016.

[42] S. Sauvage, P. Boucaud, F. H. Julien, J. M. Gérard, and J. Y. Marzin, "Infrared spectroscopy of intraband transitions in self-organized InAs/GaAs quantum dots," *J. Appl. Phys*., vol. 82, no. 7, pp. 3396-3401, Oct.1997.

[43] R. Kumar, Y. Maidaniuk, S. K. Saha, Y. I. Mazur, and G. J. Salamo, "Evolution of InAs quantum dots and wetting layer on GaAs (001): Peculiar photoluminescence near onset of quantum dot formation," *J. Appl. Phys*., vol. 127, no. 6, pp. 065306, Feb. 2020.

[44] I. Vurgaftman, J. R. Meyer, and L. R. Ram-Mohan, "Band parameters for III–V compound semiconductors and their alloys," *J. Appl. Phys*., vol. 89, no. 11, pp. 5815-5875, Jan. 2001.

[45] M. Burgelman, P. Nollet, and S. Degrave, "Modelling polycrystalline semiconductor solar cells," *Thin Solid Films*, vol. 361, pp. 527-532, Fev. 2000.

[46] G. L. Gray, "The physics of the solar cells," in *Handbook of Photovoltaic Science and Engineering*, 2nd ed., UK: Wiley, 2011, pp. 109-116.